Intermediate-energy Coulomb excitation of 104 Sn: Moderate E2 strength decrease approaching 100 Sn

P. Doornenbal, S. Takeuchi, N. Aoi, M. Matsushita, A. Obertelli, D. Steppenbeck, H. Wang, L. Audirac, H. Baba, P. Bednarczyk, et al.

PHYSICAL REVIEW C **90**, 061302(R) (2014)

Intermediate-energy Coulomb excitation of ^{104}Sn: Moderate $E2$ strength decrease approaching ^{100}Sn

P. Doornenbal,[1,*] S. Takeuchi,[1] N. Aoi,[2] M. Matsushita,[3,4] A. Obertelli,[5] D. Steppenbeck,[3] H. Wang,[1,6] L. Audirac,[5] H. Baba,[1] P. Bednarczyk,[7] S. Boissinot,[5] M. Ciemala,[7,†] A. Corsi,[5] T. Furumoto,[8] T. Isobe,[1] A. Jungclaus,[9] V. Lapoux,[5] J. Lee,[1] K. Matsui,[10] T. Motobayashi,[1] D. Nishimura,[11] S. Ota,[3] E. C. Pollacco,[5] H. Sakurai,[1,10] C. Santamaria,[5] Y. Shiga,[4] D. Sohler,[12] and R. Taniuchi[10]

[1]*RIKEN Nishina Center, Wako, Saitama 351-0198, Japan*
[2]*Research Center for Nuclear Physics, Osaka University, Ibaraki, Osaka 567-0047, Japan*
[3]*Center for Nuclear Study, University of Tokyo, RIKEN Campus, Wako, Saitama 351-0198, Japan*
[4]*Department of Physics, Rikkyo University, Toshima, Tokyo 172-8501, Japan*
[5]*CEA Saclay, Service de Physique Nucléaire, F-91191 Gif-sur-Yvette, France*
[6]*State Key Laboratory of Nuclear Physics and Technology, Peking University, Beijing 100871, China*
[7]*Niewodniczanski Institute of Nuclear Physics, Polish Academy of Sciences, 31-342 Krakow, Poland*
[8]*National Institute of Technology, Ichinoseki College, Ichinoseki-shi 021-8511, Japan*
[9]*Instituto de Estructura de la Materia, CSIC, E-28006 Madrid, Spain*
[10]*Department of Physics, University of Tokyo, Bunkyo, Tokyo 113-0033, Japan*
[11]*Department of Physics, Tokyo University of Science, Noda, Chiba 278-8510, Japan*
[12]*Institute for Nuclear Research of the Hungarian Academy of Sciences, Debrecen, H-4001, Hungary*

(Received 13 May 2013; revised manuscript received 21 August 2014; published 12 December 2014)

The reduced transition probability $B(E2)\uparrow$ of the first excited 2^+ state in the nucleus ^{104}Sn was measured via Coulomb excitation in inverse kinematics at intermediate energies. A value of 0.173(28) e^2b^2 was extracted from the absolute cross section on a Pb target. Feeding contributions in ^{104}Sn from higher lying states were estimated by a reference measurement of the stable ^{112}Sn. Corresponding only to a moderate decrease of excitation strength relative to the almost constant values observed in the proton-rich, even-A $^{106-114}$Sn isotopes, present state-of-the-art shell-model predictions, which include proton and neutron excitations across the $N = Z = 50$ shell closures as well as standard polarization charges, underestimate the experimental findings.

DOI: 10.1103/PhysRevC.90.061302 PACS number(s): 21.60.Cs, 23.20.Js, 25.70.De, 27.60.+j

Across the Segré chart of nuclei, the tin isotopes take an eminent position. Besides containing the longest chain of isotopes in between two doubly magic nuclei, in this case ^{100}Sn and ^{132}Sn, accessible to nuclear structure research, the valley of stability against β decay crosses this chain at midshell. This allows for systematic studies of basic nuclear properties from very proton-rich $N = Z$ to very neutron-rich nuclei. Of high interest in this context is the robustness of the proton $Z = 50$ shell closure when the $N = 50,82$ magic numbers are approached. Experimentally, the $Z = 50$ correlated gap size can be inferred from mass measurements when data from neighboring isotones are available. The magnitude of the proton gap is well known for neutron-rich nuclei beyond the end of the major shell and shows a maximum for ^{132}Sn [1]. On the proton-rich side, however, experimental information is more scarce and only indirect evidence for a good $Z = 50$ shell closure exists, e.g., the large Gamov-Teller strength observed in the β decay of ^{100}Sn [2].

Complementary shell evolution probes can be obtained from the $2^+_1 \rightarrow 0^+_{gs}$ transition energies, $E(2^+_1)$, and their respective reduced transition probabilities $B(E2; 0^+_{g.s.} \rightarrow 2^+_1)$, in short $B(E2)\uparrow$. While the $E(2^+_1)$ values of the tin isotopes between ^{100}Sn and ^{132}Sn are well established and exhibit only very little variation—the highest value is 1.472 MeV for ^{102}Sn, the lowest is 1.132 MeV for ^{124}Sn [3,4]—the $B(E2)\uparrow$ transition strengths follow a different pattern. The *a priori* expectation is a curve showing maximum collectivity at midshell and smoothly decreasing towards the shell closures, reflecting the number of particles times the number of holes available within the major shell. This perception is put on a formal base for a single j shell by the seniority scheme (see, e.g., Ref. [5]), which predicts constant $E(2^+_1)$ excitation energies and a parabolic pattern for the transition strengths. It has been shown that these key characteristics remain valid in the generalized seniority scheme as long as the orbits within the major shell are filled with the same rate, while for different level occupancies a shallow minimum for the $B(E2)\uparrow$ values can be obtained at midshell [6].

In recent years, several experimental findings generated large interest regarding the $E2$ strengths pattern in the tin isotopes. While the neutron-rich isotopes with $A = 126,128,130$ follow the anticipated trend of smoothly decreasing $B(E2)\uparrow$ values towards the major shell closure [7,8] well described by large-scale shell-model (LSSM) calculations [9,10], the proton-rich nuclei take a different path. Commencing with the stable $A = 114$ isotope a steadily growing deviation from the shell-model expectations was observed with almost constant $B(E2)\uparrow$ values for the $A = 106$–112 isotopes [9–14]. Conversely, the relativistic quasiparticle random phase

*pieter@ribf.riken.jp
†Present address: Grand Accélérateur National d'Ions Lourds, CEA/DSMCNRS/IN2P3, F-14076 Caen Cedex 5, France.

approximation (RQRPA) calculations presented in Ref. [15] agree well for proton-rich nuclei but underestimate $B(E2)\uparrow$ values for $A = 112$–124. This triggered a revisit of the stable tin isotopes via direct lifetime measurements, yielding generally lower $E2$ transition strengths than the adopted values given in Ref. [4] and even a local minimum for the midshell $A = 116$ nucleus [16].

While the $B(E2)\uparrow$ value of ^{102}Sn remains missing for a complete pattern of the tin isotopes within the major shell, a first attempt for ^{104}Sn with limited statistics has recently been made [17]. The result of 0.10(4) e^2b^2 indicates a steep decrease of excitation strength in agreement with LSSM calculations. In a second measurement, a considerably larger value of 0.180(37) e^2b^2 was obtained [18]. In order to ameliorate the experimental situation, a new measurement of the 2_1^+ transition strength in ^{104}Sn is desirable. Here, we report on the first $B(E2)\uparrow$ extraction in the unstable, proton-rich tin nuclei from absolute Coulomb excitation cross sections. Previously deduced values relied on target excitation at "safe" [10,11] and intermediate [12] energies or used an isotope with known excitation strength as normalization [9,17,18]. In fact, all reported values from intermediate-energy Coulomb excitation measurements above 100 MeV/nucleon rely on the latter method [9,19,20] and so far no attempt has been made to determine absolute cross sections at these high energies. Therefore, in the present work the stable ^{112}Sn isotope, which has a known $B(E2)\uparrow$ value, was Coulomb excited as well in order to validate the method.

The experiment was performed at the Radioactive Isotope Beam Factory, operated by the RIKEN Nishina Center and the Center for Nuclear Study of the University of Tokyo. A ^{124}Xe primary beam was accelerated up to an energy of 345 MeV/nucleon and impinged on a 3-mm-thick Be production target at the F0 focus of the BigRIPS fragment separator [21]. The $B\rho - \Delta E - B\rho$ method was applied to select and purify secondary beams of ^{104}Sn and ^{112}Sn in two subsequent measurements. The beam cocktail compositions were identified event by event. An ionization chamber located at the focal point F7 measured the energy loss ΔE, yielding the fragments' element number Z. The combination of position and angle measurements at the achromatic focal point F3 and the dispersive focal point F5 with parallel plate avalanche counters (PPAC) [22] and a time-of-flight (TOF) measurement with two plastic scintillators placed at the focal points F3 and F7 enabled the deduction of the mass-to-charge ratio A/Q. For the ^{104,112}Sn secondary beams, momentum acceptances were 2.2% and 0.9%, respectively.

The secondary beams were transported to the focal point F8, where a 557 mg/cm^2 thick Pb target was inserted to induce Coulomb excitation reactions. At midtarget, the secondary beam energies were 131 and 154 MeV/nucleon for the ^{104,112}Sn fragments. In order to enhance the number of tin fragments in the fully stripped charge state, 6 mg/cm^2 thick aluminum foil was placed behind the reaction target. Scattering angles were determined with two PPACs located 1430 and 930 mm upstream and one PPAC located 890 mm downstream from the secondary target. The PPACs' position resolution in X and Y was 1 mm (σ), allowing for a scattering angle reconstruction resolution of about 6 mrad, while an angular straggling of 6–8 mrad was calculated with the ATIMA code [23]. Grazing angles, calculated using the formulas given in Ref. [24], were 28 and 23 mrad for ^{104,112}Sn and their respective energies in front of the reaction target. Due to the scattering angle resolution and the angular straggling, a cut on "safe" angles would have led to a loss of a large fraction of the γ-ray yield. Therefore, no angular cut was applied and contributions from nuclear excitations were determined from inelastic scattering on a 370 mg/cm^2 thick carbon target.

To detect γ rays from the $2_1^+ \rightarrow 0_{gs}^+$ transitions, the reaction target was surrounded by the DALI2 array [25]. It consisted of 186 NaI(Tl) detectors, covering center-of-crystal angles from 19 to 150 deg. The efficiency of the DALI2 spectrometer was measured with ^{60}Co and ^{88}Y stationary sources and agreed within 5% to simulations using GEANT4 [26]. For the 1.33-MeV γ ray emitted by the stationary ^{60}Co source, a full energy peak (FEP) detection efficiency of 14% and an energy resolution of 6% (FWHM) were measured for the full array. Radiation arising from secondary bremsstrahlung produced from the ions' deceleration in the reaction target was the anticipated main source of background. Therefore, the beam pipe at the F8 focus was enclosed by 1-mm lead and 1-mm tin shields. In addition, only forward-angle detectors in the rest frame were analyzed. After Doppler shift correction for a 1.26-MeV γ ray emitted in flight, values of 10% and 8% (FWHM) were expected for the FEP efficiency and energy resolution, respectively.

Reaction products were identified behind the reaction target by the ZeroDegree spectrometer [21], using the previously described $\Delta E - B\rho$–TOF method from focus F8 to focus F11. Angular acceptances were ±30 mrad vertically and ±45 mrad horizontally for particles passing ZeroDegree with the central momentum. Figure 1 displays the particle identification plot for the ^{104}Sn setting, which exhibits three charge states. Including efficiencies of 83 and 76% for scattering angle determination, 180 and 920 particles per second of ^{104,112}Sn ejectiles were detected in the ZeroDegree spectrometer in their fully stripped charge state. Figure 2 displays the γ-ray spectra measured in coincidence with fully stripped ^{104,112}Sn ions detected in BigRIPS and ZeroDegree after applying the

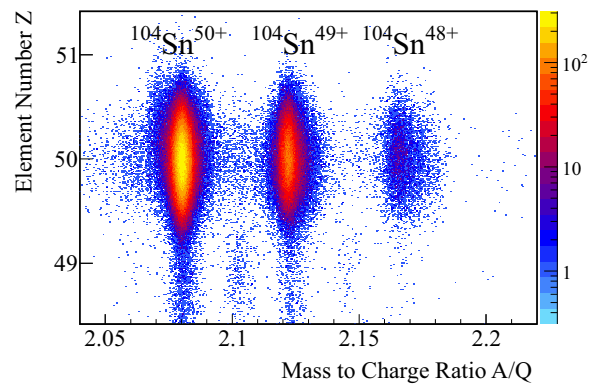

FIG. 1. (Color online) Particle identification plot behind the secondary target using the ZeroDegree beam line detectors. A gate was applied on incoming ^{104}Sn particles. Three different charge states are visible for the ^{104}Sn ejectiles.

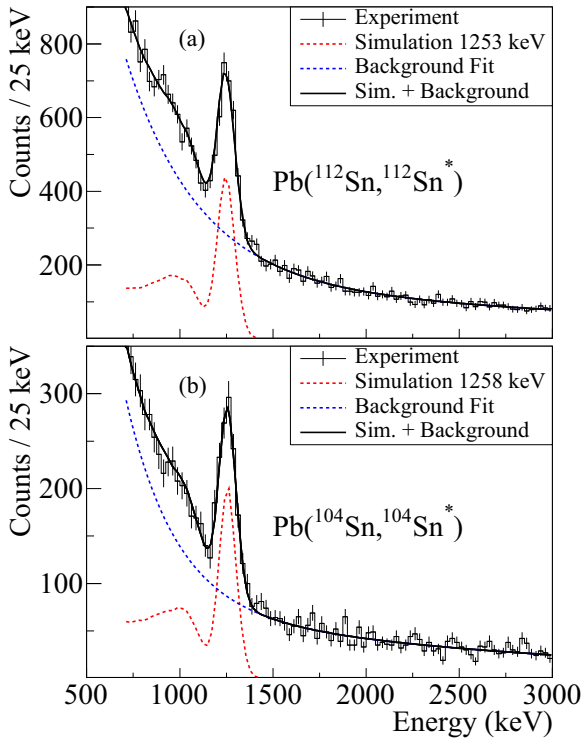

FIG. 2. (Color online) Doppler-corrected γ ray energy spectra following Coulomb excitation of fully stripped ^{112}Sn (a) and ^{104}Sn (b) ejectiles detected in coincidence with the BigRIPS and ZeroDegree spectrometers. Intensities were determined by fitting the observed line shapes with simulated response functions (red dotted [peak]) on top of two exponentials for the background (blue dotted [smooth curve]). The resulting curves are shown by the solid lines.

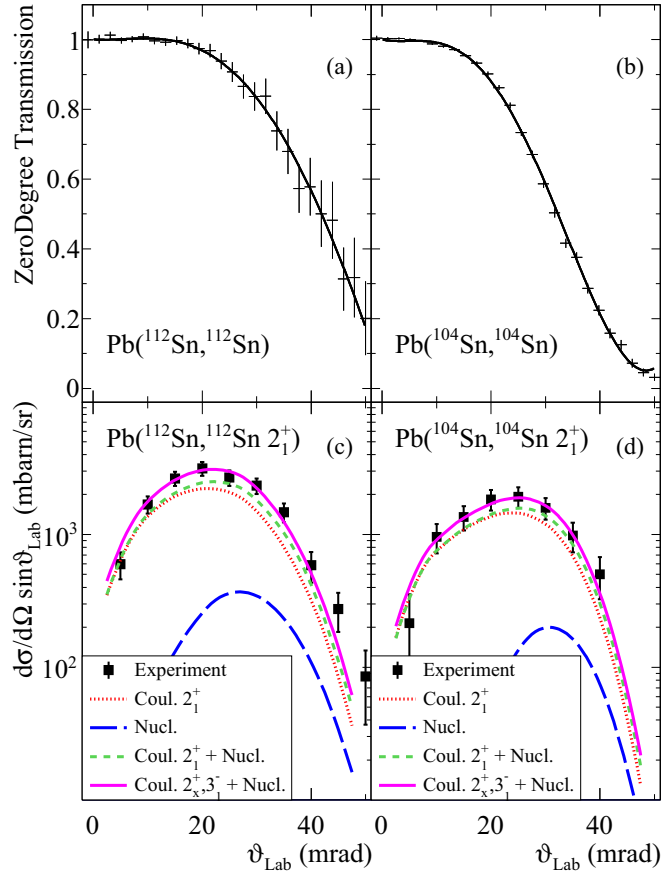

FIG. 3. (Color online) The two top panels display the ZeroDegree transmission as function of the scattering angle for ^{112}Sn (a) and ^{104}Sn (b) on the Pb target, and in the two bottom panels the differential inelastic scattering cross sections are shown for ^{112}Sn (c) and ^{104}Sn (d). The calculated distributions are Coulomb excitation of the 2^+_1 state (red [gray] dotted line), nuclear excitation (blue [gray] long-dashed line), and the sum of both (green [gray] short-dashed line). For the magenta (gray) solid lines 3^-_1 and 2^+ feeding from higher lying states was added to match the observed total cross sections in ^{104,112}Sn. See text for details.

Doppler shift correction. The two transitions were observed at 1258(6) and 1253(6) keV, close to the literature values of 1260 and 1257 keV [4]. The intensities were determined by fitting the experimentally observed spectra with simulated response functions on top of two exponentials for the background.

Measured inelastic cross sections $\sigma_{2^+_1}$ are composed of contributions from nuclear excitation (σ_n), Coulomb excitation to the 2^+_1 state (σ_c), and feeding from Coulomb excitation of higher lying states (σ_f). Thus, a measured cross section on the Pb target can be converted to a $B(E2)\uparrow$ value only if σ_n and σ_f are quantified. In addition, the ZeroDegree angular acceptance depends on the momentum distribution of the secondary beam and has to be corrected for. For the inelastic scattering of the ^{104,112}Sn isotopes on the carbon target, cross sections to the 2^+_1 state of 28(3) and 46(4) mbarn were measured, which include feeding contributions. Here, it is sufficient to determine the nuclear contributions yielding an "effective" deformation length δ that can be applied in calculations of σ_n for the lead target, assuming that the nuclear excitation patterns are similar. In order to extract δ, optical potentials were derived as described in Ref. [27] using the microscopic folding model with the complex G-matrix interaction CEG07 [28,29] and the density presented in Ref. [30]. The experimental cross sections on carbon were reproduced with the DWEIKO code [31] by selecting nuclear vibrational excitations, the derived optical potentials, and deformation lengths of $\delta = 0.32(2)$ and 0.44(3) fm for ^{104,112}Sn. For inelastic scattering of ^{112}Sn on the Pb target, the cross section to the 2^+_1 state was $\sigma_{2^+_1} = 479(37)$ mbarn, while a cross section of $\sigma_n + \sigma_c = 395(21)$ mbarn was expected from DWEIKO calculations. The errors included in the expectation value originated from the $B(E2)\uparrow$ value of 0.242(8) e^2b^2 [4,14] (13 mbarn), the derived "effective" deformation length (5 mbarn), the angular transmission shown in Fig. 3(a) (8 mbarn), as well as approximations made in the numerical calculations (14 mbarn). Comparisons to the calculated values of Refs. [32,33] made with different codes showed agreement within on average 4%, motivating the latter error on the calculations. From the difference between measured cross section and the expectation value, a feeding contribution of $\sigma_f = 84(43)$ mbarn was determined. Measured and deduced cross sections are summarized in Table I.

Feeding can be attributed to single-step Coulomb excitations to higher lying states and subsequent decay via the 2^+_1

TABLE I. Summary of observed and calculated cross sections in mbarn for the 2_1^+ state in ^{104,112}Sn.

Target	^{104}Sn	^{112}Sn
Pb	289(30)	479(37)
C	28(3)	46(4)
Decomposition for Pb target		
σ_f	41(21)	84(43)
$\sigma_c + \sigma_n$	248(36)	395(21)

state, while multistep excitations play only a minor role at intermediate energies. For example, the $B(E3)\uparrow$ value to the 3_1^- state at 2355 keV in ^{112}Sn has a strength of 0.087(12) e^2b^3 [34] and decays through the 2_1^+ state. This translates to a feeding contribution of 10(2) mbarn. For $E2$ excitations, the total strength measured in the heavier $^{116-124}$Sn isotopes between 2 and 4 MeV corresponds to about 10% of that to the first excited state [35], while no experimental information is available for 2^+ states at higher energies. Figure 3(c) displays the measured differential cross section as function of scattering angle for ^{112}Sn. It is compared to the calculated nuclear cross section, the 2_1^+ Coulomb excitation cross section, their combination, and adding the feeding from the 3_1^- and 2_x^+ states. For the latter, the feeding was adjusted to match the experimental cross section. Coulomb excitations are dominant for all scattering angles, as nuclear contributions are sizable only around the grazing angle. A larger nuclear contribution would have resulted in a maximum at the grazing angle. Additionally, only by including sizable feeding can the curve up to scattering angles of ≈20 mrad be reproduced. All calculations were convoluted with the detector resolution, the angular straggling, and the observed ZeroDegree scattering angle transmission.

The observed feeding contributions in ^{112}Sn can be used to evaluate the feeding for ^{104}Sn. We follow a similar approach to the one presented in Ref. [36] for neutron-rich magnesium isotopes to determine its value. In a simple picture, feeding originates from the 3_1^- excitation and fragmentation of the $E2$ excitation strength to many 2^+ states between 2 MeV and the proton separation energy S_p (7.554(5) MeV for ^{112}Sn and 4.286(11) MeV for ^{104}Sn [1]). Assuming an uniform $E2$ excitation strength distribution in this region and the same $E3$ excitation strength, correcting for the angular transmission shown in Fig. 3(b) results in a feeding of $\sigma_f = 41(21)$ mbarn for ^{104}Sn, mainly due to the lower S_p value. This estimation may be corroborated by a higher peak-to-background ratio for ^{104}Sn despite a lower total cross section, showing that fewer high lying excited states are populated.

For inelastic scattering of ^{104}Sn on the Pb target, a cross section of $\sigma_{2_1^+} = 289(30)$ mbarn was measured. Taking the previously determined nuclear contributions and the feeding into account, a $B(E2)\uparrow$ of 0.173(28) e^2b^2 was deduced. Note that due to the lower beam energy and the reduced scattering angle acceptance, nuclear contributions were significantly suppressed, as can be seen in the differential cross section in Fig. 3(d). The new $B(E2)\uparrow$ value is displayed in Fig. 4 together

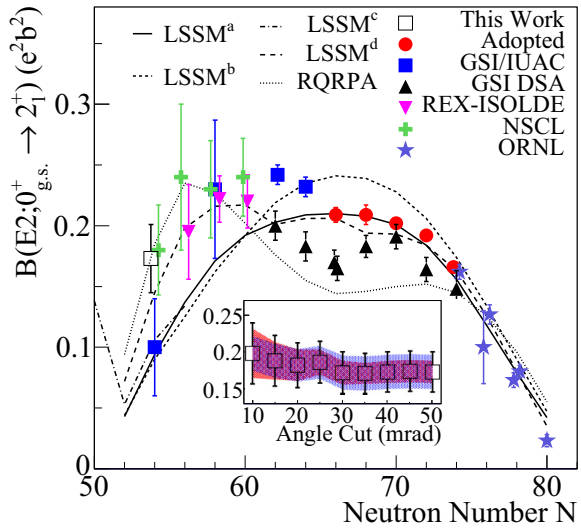

FIG. 4. (Color online) Experimental $B(E2)\uparrow$ values for even-mass Sn isotopes in between the doubly magic ^{100}Sn and ^{132}Sn nuclei [4,7–14]. Results from LSSM calculations using different inert cores and effective charges and the RQRPA calculation are shown for comparison. The inset shows extracted $B(E2)\uparrow$ for ^{104}Sn of the present work when different cuts on the scattering angle are applied. Statistical and systematic errors contributing to the total error are shown individually by the hatched areas. See text for details.

with known data in between the two doubly magic tin nuclei. It is noteworthy that extracted $B(E2)\uparrow$ values from the present experiment are robust against applying scattering angle cuts, as shown in the inset of Fig. 4. Systematic and statistical errors are shown individually, the latter dominating when applying cuts on small angles and the former for large angles. Our result is in agreement with the 0.180(37) e^2b^2 obtained in Ref. [18] with largely overlapping error bars, but deviates significantly from the value of 0.10(4) e^2b^2 obtained in Ref. [17]. It corresponds to only about 30% excitation strength decrease compared to the even-A $^{106-114}$Sn isotopes and confirms that the reduction is much more shallow than first suggested.

Various $B(E2)\uparrow$ calculations of the tin isotopes have been recently presented [6,9,10,15,17,18,37,38]. owing to the experimental progress. Very instructive are the LSSM calculations presented with the first intermediate-energy Coulomb excitation experiment on proton-rich tin isotopes [9]. Within that work, two sets of $B(E2)\uparrow$ calculations were performed, using ^{100}Sn and ^{90}Zr as inert cores, respectively, and an effective interaction derived from the CD-Bonn potential [39]. The former, denoted LSSM[a], used a neutron model space with the $1d_{5/2}$, $0g_{7/2}$, $1d_{3/2}$, $2s_{1/2}$, and $0h_{11/2}$ orbitals, and the latter, denoted LSSM[b], contained the proton $0g_{9/2}$, $0_{g7/2}$, $1d_{5/2}$, $1d_{3/2}$, and $2s_{1/2}$ (gds) orbitals as well. Neutron effective charges of $e_\nu = 1.0e$ were used for the ^{100}Sn core calculations to compensate for the neglect of proton excitations across the $Z = 50$ shell while the ^{90}Zr core calculations allowed up to four-particle–four-hole proton excitations and used "standard" neutron and proton effective charges of $e_\nu = 0.5e$ and $e_\pi = 1.5e$. The results are added in Fig. 4 to the experimental values between the two doubly magic nuclei and yield inverted

parabola in agreement with the neutron-rich nuclei but fail to reproduce the $B(E2)\uparrow$ enhancement for proton-rich nuclei.

In the most recent shell-model prediction, denoted LSSM[c] in Fig. 4, the calculations were expanded to a ^{90}Zr core and a gds model space, thereby allowing neutron as well as proton excitations across the $N = Z = 50$ gap [17]. The standard effective charges were used and truncation was applied depending on the nuclei's neutron number due to computational limits. However, the inclusion of neutron excitations across the $N = 50$ gap augmented the $B(E2)\uparrow$ values only slightly. For ^{104}Sn, a value of about 0.1 e^2b^2 is predicted, well below our experimental finding, and also the experimental $B(E2)\uparrow$ values for ^{106}Sn are underestimated.

Different suggestions to break the symmetry in the theoretical $B(E2)\uparrow$ pattern have been made ranging from refined tuning of the proton-neutron monopoles [9,11], inclusion of excitation across the $N = 50$ shell [9], a $N = 50$ shell gap reduction [10], to simply using two different sets of single-particle levels and effective charges for the lower and upper half of the shell [37]. In an alternative approach that included the neutron gds and $0h_{11/2}$ orbitals as model space and single-particle energies fitted to experimental data [40], isospin-dependent effective charges as proposed by Bohr and Mottelson [41] were introduced into the calculations [38]. The neglect of proton excitations was compensated by normalizing the effective charges to $e_\nu = 1.0e$ in the middle of the shell for ^{116}Sn, resulting in $e_\nu > 1.0e$ ($e_\nu < 1.0e$) in the lower (upper) half of the shell. Indeed, a good overall agreement is observed for very neutron- and proton-rich nuclei, as shown in Fig. 4 by LSSM[d]. However, the collectivity increase on the proton-rich side commences later than observed in experiments [13,14,16] and the large effective charges are also coincident with the correlated proton gap minimum around ^{108}Sn (see, e.g., Fig. 4 of Ref. [13]).

In combination with the neglect of proton excitations, this effective charge adjustment can therefore only be regarded as an interim solution until sufficient computing power becomes available. The importance of proton excitations across the $Z = 50$ shell for the $B(E2)\uparrow$ pattern could be in principle inferred from the difference in "matter" deformation lengths obtained from the comparison of nuclear and electrical excitations. In the present study the analysis of carbon-induced excitations within a vibrational model yields an "effective" deformation length of $\delta = 0.32(2)$ fm, whereas the $B(E2)\uparrow$ value leads to $\delta_c = 0.59(9)$ fm following the model-dependent formula $\delta_c = (4\pi/3eZR_0)B(E2)\uparrow^{1/2}$ and $R_0 = 1.2A^{1/3}$ fm [4]. Firm conclusions should be drawn from a microscopic analysis of proton-induced inelastic cross sections [42].

In summary, a $B(E2)\uparrow$ value of 0.173(28) e^2b^2 was measured for ^{104}Sn in intermediate-energy Coulomb excitation. The drop in excitation strength is much smoother than obtained in Ref. [17] and cannot be reproduced by present LSSM calculations using standard effective charges as well as proton and neutron excitation across the $N = Z = 50$ shell. Moreover, it was demonstrated that given the significant scattering angle resolution and angular straggling at energies well above 100 MeV/nucleon, nuclear excitation should be explicitly taken into account in $B(E2)\uparrow$ determinations rather than suppressed in an inaccurate angular cut. Feeding from higher lying states cannot be neglected but can be determined from known $B(E2)\uparrow$ values. A simple scaling of measured cross sections for the ^{104,112}Sn pair would have led to a 7% lower $B(E2)\uparrow$ assignment for ^{104}Sn. This may be acceptable for many low-statistics experiments, but for future high-accuracy absolute cross-section measurements at energies well above 100 MeV/nucleon we suggest calibration runs of nuclei with known $B(E2)\uparrow$ values on a high-Z target and nuclear excitation on a low-Z target. Such an approach allows for the use of very thick reaction targets and thus gives access to more exotic nuclei.

We thank the RIKEN Nishina Center Accelerator Group for providing the high ^{124}Xe primary beam intensity and the BigRIPS team for preparing high-purity secondary beams for the isotopes of interest. We acknowledge financial support from the Spanish Ministerio de Ciencia e Innovación under Contracts FPA2009-13377-C02-02 and FPA2011-29854-C04-01, the OTKA under Contract No. K100835, and the European Research Council through the ERC Starting Grant MINOS-258567.

[1] M. Wang, G. Audi, A. Wapstra, F. Kondev, M. MacCormick, X. Xu, and B. Pfeiffer, Chin. Phys. C **36**, 1603 (2012).
[2] C. Hinke *et al.*, Nature (London) **486**, 341 (2012).
[3] M. Lipoglavsek *et al.*, Z. Phys. A **356**, 239 (1996).
[4] S. Raman, C. W. Nestor Jr., and P. Tikkanen, At. Data Nucl. Data Tables **78**, 1 (2001).
[5] R. Casten, *Nuclear Structure from a Simple Perspective* (Oxford University Press, Oxford, 2001).
[6] I. Morales, P. V. Isacker, and I. Talmi, Phys. Lett. B **703**, 606 (2011).
[7] D. Radford *et al.*, Nucl. Phys. A **746**, 83 (2004).
[8] J. Allmond *et al.*, Phys. Rev. C **84**, 061303(R) (2011).
[9] A. Banu *et al.*, Phys. Rev. C **72**, 061305 (2005).
[10] A. Ekström *et al.*, Phys. Rev. Lett. **101**, 012502 (2008).
[11] J. Cederkäll *et al.*, Phys. Rev. Lett. **98**, 172501 (2007).
[12] C. Vaman *et al.*, Phys. Rev. Lett. **99**, 162501 (2007).
[13] P. Doornenbal *et al.*, Phys. Rev. C **78**, 031303 (2008).
[14] R. Kumar *et al.*, Phys. Rev. C **81**, 024306 (2010).
[15] A. Ansari, Phys. Lett. B **623**, 37 (2005).
[16] A. Jungclaus *et al.*, Phys. Lett. B **695**, 110 (2011).
[17] G. Guastalla *et al.*, Phys. Rev. Lett. **110**, 172501 (2013).
[18] V. Bader *et al.*, Phys. Rev. C **88**, 051301(R) (2013).
[19] A. Bürger *et al.*, Phys. Lett. B **622**, 29 (2005).
[20] T. Saito *et al.*, Phys. Lett. B **669**, 19 (2008).
[21] T. Kubo *et al.*, Prog. Theor. Exp. Phys. **2012**, 3C003 (2012).
[22] H. Kumagai, A. Ozawa, N. Fukuda, K. Sümmerer, and I. Tanihata, Nucl. Instrum. Meth. A **470**, 562 (2001).
[23] ATIMA code, http://web-docs.gsi.de/~weick/atima/
[24] H. Wollersheim *et al.*, Nucl. Instrum. Meth. A **537**, 637 (2005).
[25] S. Takeuchi, T. Motobayashi, Y. Togano, M. Matsushita, N. Aoi, K. Demichi, H. Hasegawa, and H. Murakami, Nucl. Instr. Meth. A **763**, 596 (2014).

[26] S. Agostinelli *et al.*, Nucl. Instr. Meth. A **506**, 250 (2003).
[27] T. Furumoto, W. Horiuchi, M. Takashina, Y. Yamamoto, and Y. Sakuragi, Phys. Rev. C **85**, 044607 (2012).
[28] T. Furumoto, Y. Sakuragi, and Y. Yamamoto, Phys. Rev. C **78**, 044610 (2008).
[29] T. Furumoto, Y. Sakuragi, and Y. Yamamoto, Phys. Rev. C **80**, 044614 (2009).
[30] L. Chamon *et al.*, Phys. Rev. C **66**, 014610 (2002).
[31] C. A. Bertulani, C. M. Campbell, and T. Glasmacher, Comp. Phys. Com. **152**, 317 (2003).
[32] C. A. Bertulani, G. Cardella, M. De Napoli, G. Raciti, and E. Rapisarda, Phys. Lett. B **650**, 233 (2007).
[33] H. Scheit, Alexandra Gade, T. Glasmacher, and T. Motobayashi, Phys. Lett. B **659**, 515 (2008).
[34] N. Jonsson, A. Backlin, J. Kantele, R. Julin, M. Luontama, and A. Passoja, Nucl. Phys. A **371**, 333 (1981).
[35] J. Bryssinck *et al.*, Phys. Rev. C **61**, 024309 (2000).
[36] V. Chisté *et al.*, Phys. Lett. B **514**, 233 (2001).
[37] H. Jiang, Y. Lei, G. E. Fu, Y. M. Zhao, and A. Arima, Phys. Rev. C **86**, 054304 (2012).
[38] T. Bäck, C. Qi, B. Cederwall, R. Liotta, F. G. Moradi, A. Johnson, R. Wyss, and R. Wadsworth, Phys. Rev. C **87**, 031306(R) (2013).
[39] R. Machleidt, Phys. Rev. C **63**, 024001 (2001).
[40] C. Qi and Z. X. Xu, Phys. Rev. C **86**, 044323 (2012).
[41] A. Bohr and B. Mottelson, *Nuclear Structure*, Vol. 2 (Benjamin, New York, 1975).
[42] A. Corsi *et al.* (unpublished).